

Article

Composition Distribution, Damping and Thermal Properties of the Thickness-Continuous Gradient Epoxy/Polyurethane Interpenetrating Polymer Networks

Xuesong Lv ¹, Zhixiong Huang ^{1,*}, Minxian Shi ^{1,*}, Yun Fan ² and Guanbin Gao ^{3,*}

¹ Key Laboratory of Advanced Technology for Specially Functional Materials, Ministry of Education, Wuhan University of Technology, Wuhan 430070, China; wryd@whut.edu.cn

² College of Foreign Languages and Literature, LuoJia College, Wuhan University, Wuhan 430064, China; xiaofeige12121@gmail.com

³ State Key Laboratory of Advanced Technology for Materials Synthesis and Processing, Wuhan University of Technology, Wuhan 430070, China

* Correspondence: zhixiongh@whut.edu.cn (Z.H.); minxianshi@whut.edu.cn (M.S.);
gbgao@whut.edu.cn (G.G.); Tel.: +86-138-0718-0447 (Z.H.); +86-189-7142-5643 (M.S.);
+86-27-8786-0735 (G.G.)

Academic Editor: Andrew J. Ruys

Received: 23 August 2016; Accepted: 16 January 2017; Published: 30 January 2017

Abstract: A thickness gradient interpenetrating polymer network (IPN) was easily created that takes advantage of the relatively poor compatibility and curing rates discrepancy between epoxy (EP) and polyurethane (PU). Ultraviolet absorption spectrum (UV-Vis), thermogravimetric (TG), Differential scanning calorimetry (DSC), Dynamic thermomechanical analysis (DMA), Atomic force microscope (AFM) and water contact angle were adopted to characterize this IPN structure. We found that the absorption in visible light region, glass-transition temperatures (T_g), thermal decomposition temperatures (T_d) and Derjaguin–Muller–Toporov (DMT) modulus were increasing along with the gradient direction from bottom side to top side of the IPN. While the absorption in ultraviolet region and adhesion force were decreasing along with the gradient direction from bottom side to top side of the IPN. DMA analysis demonstrates that this continuous gradient IPN has a good balance between the damping temperature range and the loss factor which is suitable for using as a self-supporting damping structure.

Keywords: PU-EP IPN; gradient composite; AFM analysis; damping analysis; TG analysis

1. Introduction

Polymers have been a promising damping materials because of their good damping capacity to decrease noise and vibration within their range of glass-transition temperature (T_g) [1,2]. However, the limited damping temperature range ΔT (usually covers 20–30 °C), the low storage modulus E' (less than 1 GPa) and the mismatch between the working frequencies and actual required frequencies limit the applications of polymers as damping materials in engineering [3]. The several existing types of damping polymers (such as the polymer blend, copolymer, IPNs) have still not solved these deficiencies [4–9]. Therefore, damping polymers must be attached onto substrates to work as free damping or constrained damping structures instead of being singly used as structures until now [10–12]. However, the serious mismatching of modulus between polymers and substrates might cause some interfacial problems such as stress concentration and joint failure after periods of vibration.

Gradient materials are composites with continuous variation of properties from one side to another [13], which can decrease some shortcomings of the traditional composites, such as the abrupt changing of stress distributions at interfaces in damping structures and low resistance to temperature shocks. Since the concept of gradient materials was put forward in 1984 [14,15], lots of papers have been published [16–26]. However, the ambiguous terms “graded material”, “thickness gradient” or “bilayer material”, which can be found in literatures, are shown in Figure 1 (a detailed comparison between them can be found in Figures S1–S3).

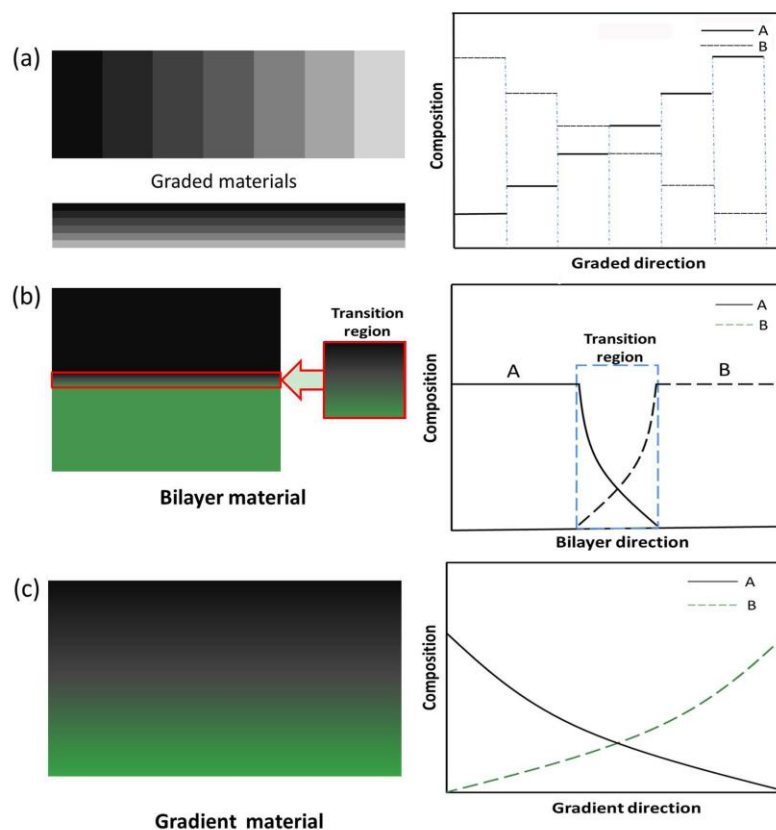


Figure 1. Schematic diagram of the graded material (a); bilayer material (b); and the continuous gradient material (c). The tonality represents the changing composition ratio. The solid curves (A) and dotted curves (B) in right side figure represent the components ratio used in composite.

Graded material (Figure 1a) is a multi-layered structure, in which the compositions change stepwise from one layer to another along a certain direction, while the compositions in each layer are homogeneous. This kind of graded material is usually generated layer by layer. In addition, the mechanical properties of composites transform orderly from each adjacent sections.

Bilayer material (Figure 1b) has a thin-inside transition zone, in which the compositions change sharply. In contrast, the compositions are homogeneous outside the transition zone. There are two different methods to prepare the bilayer material. One is casting different resins into a mold via layer by layer. In addition, the transition region is generated by molecular diffusion during the curing process. The other is using an incomplete self-stratification of resin mixture to form a thin film. Mechanical properties (e.g., storage modulus and stiffness) of this bilayer material in transition region would change sharply. The stress of this bilayer material usually concentrates in this transition zone, which will lead to adhesive failure under tensions along graded direction. Bilayer material cannot be regarded as the truly gradient material because of its limited phase interfacial transition zone.

Gradient composite, as shown in Figure 1c, has a continuous changing of compositions from one side to the other (Figure S4 and Table S1). It can be regarded as combinations of infinite ultra-thin layers,

and each layer is homogeneous in composition. The unique structure endows this kind of composites a plenty of new properties comparing to the traditional polymers. Previous works of this gradient composite mainly focused on the fabricating methods, mechanical analysis or biocompatibility [27,28]. While, the damping properties of gradient materials are still unclear. Furthermore, the fabricating processes of these gradient materials are usually complex, expensive and time-consuming [29,30].

Within the temperature region of the two T_g points of PU and EP (T_g of PU $\leq T \leq T_g$ of EP), rubbery state, glass transition region and glassy state are coexisting in the gradient composite. Because the “transition regions” in gradient composite always exist and transfer with the temperature, this gradient composite show better damping performances in various environment comparing to homogeneous polymers. In addition, the glassy state region of this composite can provide self-supporting strength and keep its own shape. This kind of structure can replace the traditional constrained damping structures when the soft side was pasted onto substrates, because the stress concentration and risk of adhesion failure will reduce with the decreasing of contact interfaces. Therefore, the gradient composite may be a promising damping material, which could be used in automobile, shipbuilding and aerospace industry.

In nature, there are many gradient structures, e.g., bamboo, squid's beak and mussel byssus [31–33]. As shown in Figure 2, in order to resist the waves, mussel possess the natural strategy to minimize interfacial stresses via byssus anchor itself onto hard rocks, and 70% of the absorbed energy can be dissipated by the byssus [34–37].

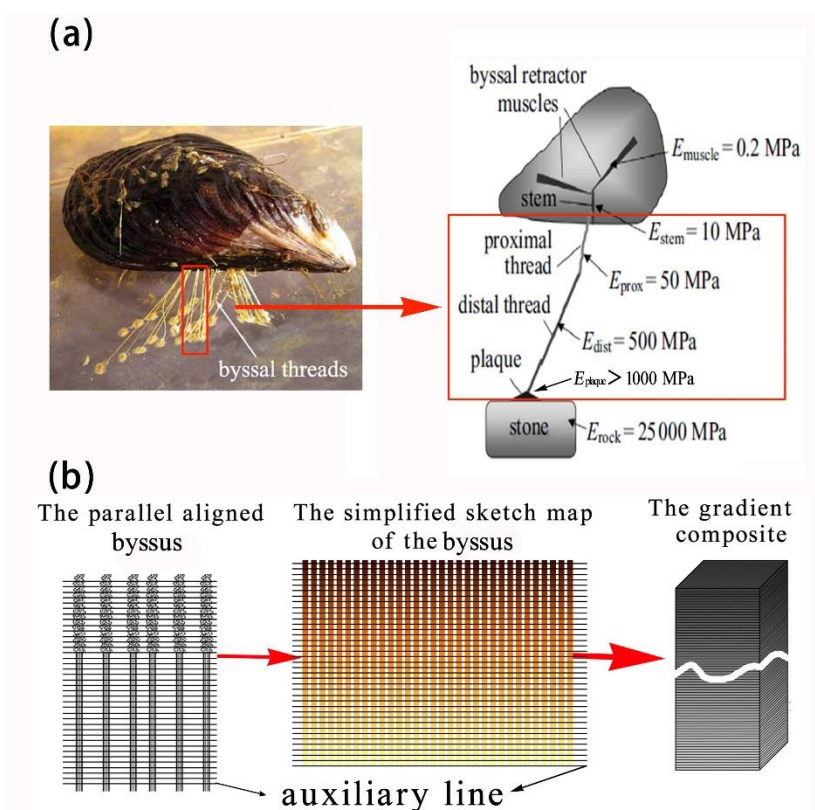


Figure 2. (a) The schematic drawing of the mussel byssus. The byssal thread is a gradient structure along the axial direction. Modulus of the plaque is higher than 1 GPa, while the modulus of the proximal threads is only around 10 MPa; (b) When byssus are parallel aligned, the close-set threads looks like a holistic structure (the gradient composite).

Inspired by natural gradient structures, we prepared a series of thickness-continuous gradient IPNs due to the relative poor compatibility and curing rates discrepancy between EP (LY-1564) and PU

(130 T). Our previous article has reported the self-gradient mechanism and the morphology of these IPNs [38]. Here we report the damping, wettability and thermal properties of this thickness-continuous gradient IPN.

2. Materials and Methods

2.1. Materials

Low viscosity epoxy LY-1564 (1200~1300 CPS, 1.06 g/cm³, 25 °C) was bought from Huntsman. Double-pack polyurethane (PU, 130 T) was purchased from Ausbond; of which component A (PU-a, 1.11 g/cm³, 25 °C) is the isocyanate, component B (PU-b, 0.98 g/cm³, 25 °C) is the polyalcohol. Mix viscosity of the double components is 1600 CPS under 25 °C. Curing agent 2,4,6-Tris (dimethylaminomethyl) phenol (DMP-30) was acquired from Shanghai Deyin Chemical Company. Solid phosphoric acid (chemical pure, sifted out through 600 mesh) was prepared from Shanghai Yunlong chemical reagent works.

2.2. Preparation of Samples

All materials were dried in a vacuum oven at 70 °C under −0.1 MPa for more than 3h before used.

Three kinds of IPN samples (the homogeneous IPN, the continuous gradient IPN and the graded one) were prepared and tested to have a detailed research of the damping performances.

For the homogeneous one (PU to EP equals to 35/65 by weight), 9.72 g (19.44%) PU-a, 7.78 g (15.56%) PU-b (according to the recommend dosage PU-a: PU-b is 5/4 by weight), 0.3 g solid phosphorus acid and 32.5 g (65.00%) EP were mixed together. After stirred for several minutes, 2.6 g DMP-30 was dropped into the mixture. Then, the colorless mixture was put into a vacuum drying oven under −0.1 MPa (15 °C) to remove bubbles after a completely stirring by a homogenizer. The mixture was then casted into the mold and cured under vacuum environment at 80 °C for 12 h. Solid phosphorus acid used here was to reduce the side reactions of isocyanate root. Size of the casting bodies is 2.17 mm × 100 mm × 100 mm.

As for the continuous gradient IPN, the liquid mixture was prepared according to the homogeneous one. However, the defoamed mixture was cured differently. The castings were horizontally placed in the vacuum oven for 24 h (−0.1 MPa, 10 °C) first, and then were postcured. Sample sizes were the same as the homogeneous IPN.

Besides, to simulate the gradient structure, a third type of specimen (the graded sample), which consists of 6 layers of h-IPN whose component ratio of PU to EP were 0/100, 6/94, 12/88, 25/75, 50/50, 100/0 separately, were made and cured at 80 °C by layer-by-layer method. Thickness of each layer was 0.4 mm.

2.3. Measurement

UV-Vis absorption of sample was carried out using an Avalight-DH-S-BAL (Avantes, Apeldoorn, The Netherlands). Fracture surfaces should be carefully polished by 5000 mesh abrasive papers using a PHOENIX 4000 lapping and polishing machine (Buehler, Lake Bluff, IL, USA) and vacuum dried before testing. Contact angles were measured using the “sessile drop method” through a Newjc2000X contact angle analyzer (POWEREACH, Shanghai, China). Contact angles were read through the Yong-Lapalace fitting & analysis software (trial version, Kino, HongKong, China). Modulus distributions (under the temperature of 20 °C) of the fractured surfaces were taken in the air with Peak Force QNM mode using the J scanner on a MultiMode8 Scanning Probe Microscopy (BRUKER, Karlsruhe, Germany) at room temperature after the absolute calibration. Fracture surface should be carefully polished according to the UV-Vis method and vacuum drying in case of breakage of the probes.

Differential scanning calorimeter (TA Q2000, TA Instruments, New Castle, DE, USA) was applied to record the glass-transition temperatures of the slices along the gradient direction. Temperature was stabilized at 80 °C for 5 min to eliminate the thermal history and then swept from −40 to

95 °C at a slope of 15 °C/min in nitrogen atmosphere (50 mL/min, aluminum crucible). After the thermal history was eliminated and the slices were rapid cooled, the second scanning curves were recorded. Thermostability (TG analysis) of casting bodies was measured by the STA449c/3/G (NETZSCH, Bavaria, Germany) with a heating rate of 10.0 °C/min (air atmosphere) from 50 to 600 °C. The DMA/STDA 861e (METTLER TOLEDOR, Zurich, Switzerland) equipment (shear mode) was used for damping analysis. Temperature ranges from −40 to 130 °C at a heating rate of 1.5 °C/min, 1 Hz. Samples size was Φ 8.79 mm \times 2.17 mm.

The self-gradient mechanism of the mixture can be found on the literature published before [38].

3. Results and Discussion

3.1. UV-Vis Absorption

Because the UV-vis absorption shows different intensities along with the gradient direction of the IPN, it can be used for detecting the gradient structure. As shown in Figure 3, after the specimen was fractured (along the direction of thickness) and well-polished, 1/8 h, 1/2 h and 7/8 h regions were selected for testing (characterizations of the gradient structure through the infrared absorption spectrum can be found in Figures S5 and S6).

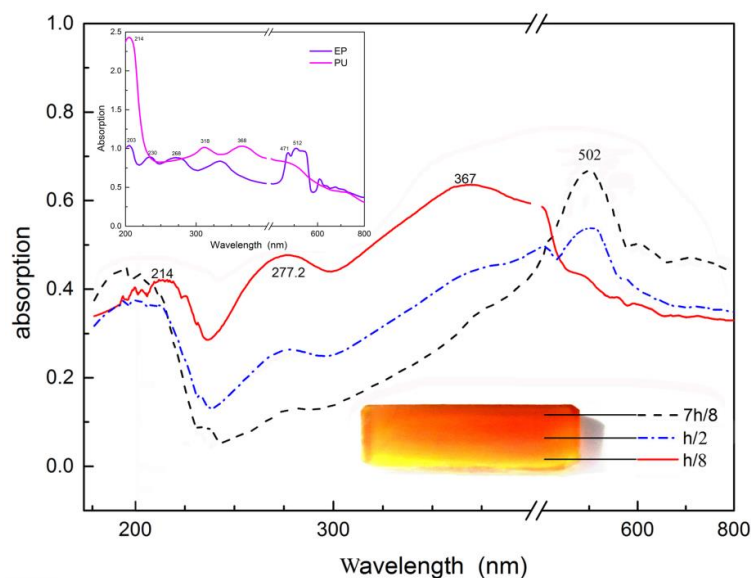


Figure 3. Ultraviolet absorption spectrum (UV-Vis) absorption spectra of the chosen regions in the gradient interpenetrating polymer network (IPN). The top left insert is the absorption spectra of PU and EP. Here “h” represents the thickness.

As shown in the top left insert figure, the peaks of 214, 318 and 368 nm can be assigned to the maximum absorption of acylamino groups, the R bond of ketone groups and the ether bonds in PU, respectively. Peaks at 203 and 230 nm should be ascribed to the maximum absorption E₂ bond and the triethylene conjugated structure of benzene rings in EP [39–41]. Besides, the absorption band between 470 and 560 nm may be attributed to the conjugated structures between tertiary amine and the benzene rings, which explain the tawny color of cured EP.

As shown in Figure 3, the chosen regions show similar absorption in the UV band. In addition, compared to PU and EP, the new peak of 277 nm in IPN could be assigned to the inter-molecular interaction between acylamino group in PU and the alkoxy groups in EP. According to the absorption curves of h/8, h/2 and 7h/8 regions, we can find that the absorption intensities between 200 and 400 nm decrease from the bottom side to the top side of the sample. This indicates that the percentage of PU in the IPN composite is reducing along the gradient direction. In addition, the absorption of

benzene ring (203 nm) in the chosen regions of the sample implies that the layer near the top side has the maximum content of EP.

In contrast, the absorption intensities in the range of visible light are increasing along the gradient direction from the bottom side to the top side of the sample. In addition, the increasing absorption between 400 and 600 nm (the range of blue-green light) makes the gradient IPN composite show gradual loss of tawny color.

3.2. Contact Angles

Contact angles can be employed to determine the gradient structure of the IPN because EP and PU have different surface wettability [42–44]. After the fracture surface of the IPN sample was well polished using a 5000 mesh abrasive paper, contact angles between the dried gradient IPN and redistilled water were measured (Figure 4).

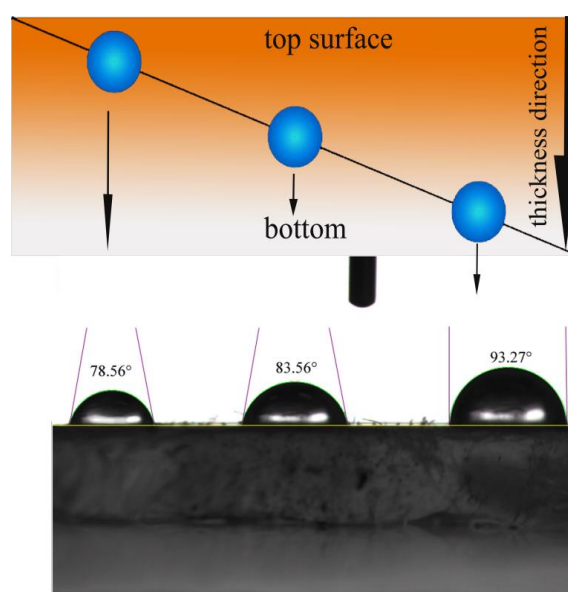


Figure 4. Water contact angles on the fracture surface of the gradient IPN. Regions are symmetrically selected along the diagonal line of the fracture surface and they are from 1/4 h, 2/4 h and 3/4 h, respectively. Here “h” represents the thickness of the IPN samples.

Our previous work have reported that the water contact angles of EP (LY-1564) and PU (130 T) are 75.42° and 110.06° , respectively. As shown in Figure 4, surface water contact angle of the IPN sample at the region of 3/4 h, 2/4 h and 1/4h are 78.56° , 83.56° and 93.27° , Which increases along with the gradient direction.

Previous reports have indicated that surface tensions imparity and curing rate discrepancy of PU and EP are the main driving force in the self-gradient process [38,45]. PU phase has higher surface tension and shorter gel time than that of EP phase in the IPN. Therefore, the earlier gelled PU phase will mainly distribute in the bottom of the IPN according to the thermodynamics, while the EP phase will be extruded to the top side of the IPN, which leads to the continues gradient distributions of the components. Thus, the water contact angle shows the same trend along the gradient direction.

3.3. DSC Analysis

To further explore the structure of the IPN, we used DSC analysis to study the changes of the glass-transition temperatures of sample slices along the gradient direction. The IPN samples are divided into 100 layers from bottom to top with a thickness of 21.5 μm per layer. We cutting them layer by layer at the temperature of -50°C by utilizing a microtome (CM1950 kryptome, Lecia Biosystem,

wetzlar, Germany). The 90th (rose), 45th (black), 15th (red) layers and a slice parallel to the gradient direction (blue) were selected for testing.

The baseline shift in DSC curve usually happens in the glass transition region of polymer due to the changes of heat capacity. As shown in the Figure 5, the T_g of the 15th, 45th and 90th layers are -16.3 , 14.1 and 51.8 °C, respectively. The glass-transition temperature increases along with the gradient direction of IPN from bottom to top. That can be explained by the content decrease of the PU phase in the IPN sample. Because of the relative faster curing rate of the polyurethane, PU gels earlier, and it will result in the IPN structure with PU as its main body (fewer EP content) near the bottom side. In contrast, the top side is the IPN structure with EP as its main body. The DSC curve of the whole slice appears as a multi-sidestep shape; that can be explained by the gradient distribution of the PU phase along the thickness direction in the IPN sample.

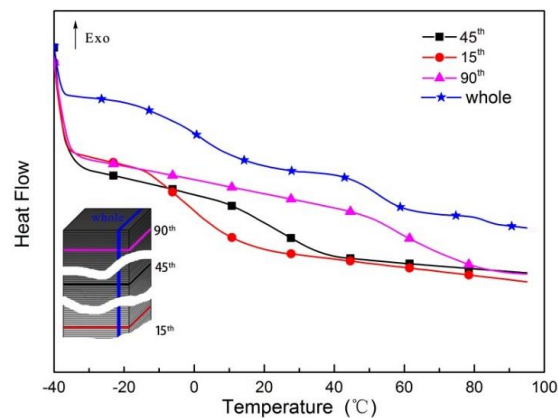


Figure 5. Differential scanning calorimetry (DSC) analysis of the slices selected from the gradient IPN. Temperature sweeps from -40 to 95 °C at a slope of 15 °C/min in nitrogen atmosphere (50 mL/min).

3.4. TG Analysis

To investigate the thermo stability of sample slices in different regions of IPN sample, 1mm layers of the 75th, 50th, 25th, EP and PU were selected for TG analysis (Figure 6).

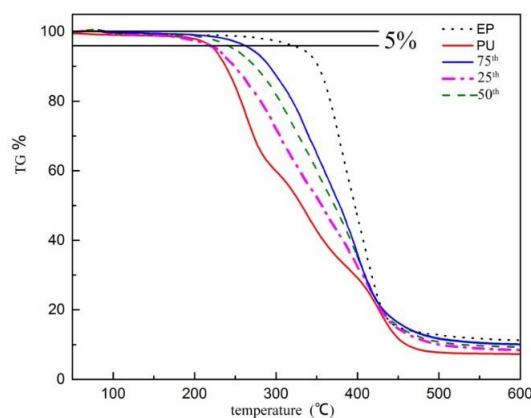


Figure 6. Thermogravimetric (TG) curves of epoxy (EP), polyurethane (PU) and the chosen layers from the gradient IPN sample. Heating rate: 10.0 °C/min, air atmosphere.

The rigidity of polymer chains and the crosslinking density of cross-linked polymers determine the thermal decomposition temperature (T_d). Due to EP (LY-1564) is mainly composed of rigid chains such as benzene ring and carbon-oxygen bond, it has the highest T_d (about 330 °C) and the largest residual mass (about 17%) at the temperature of 470 °C.

In contrast, PU is mainly composed of ether bonds. Because of these weaker bonds and the lower crosslinking density, the thermal decomposition temperature of PU is around 210 °C. The thermal decomposition process of PU can be separated into 3 stages: 210~280 °C, 300~380 °C and 400~450 °C. The first stage represents the decomposition of the C–O bond as well as the generation of isocyanate and polyhydric alcohols. Parts of the generated isocyanate would volatilize which led to the weight loss in the first step. Meanwhile, the rest isocyanate would be self-aggregate into dimer or trimer. The second stage is that the dimers/trimers resolve into amines, alkenes and carbon dioxide. In addition, the volatilization of these products caused the second weight loss. The first two stages lose about 55% of PU weight, which exactly equal to the percentage of the isocyanate in PU. The final stage is the pyrolysis of the polyhydric alcohols. In addition, the pyrolysis products are water and carbon dioxide. The final residual mass is about 7% of the original PU.

The thermal decomposition temperature (T_d) of the 25th, 50th and 75th slices in the IPN are 220, 247 and 268 °C, respectively. The residual weight of the 75th slice (11%) is heavier than that of the 25th (8%), and the residual weight of the 50th (10%) lies between them. This result can be explained by the decrease of PU content in the IPN along with the gradient direction from bottom to top. Meanwhile, shape of the TG curves of the gradient IPN is different from that of PU. This may be explained by the synergistic effect between PU and EP in this IPN structure.

3.5. AFM Analysis

The mechanical properties of the gradient IPN was characterized by PeakForce QNM (quantitative nanomechanical property mapping) mode on a Bruker Multi-Mode VIII AFM, which allows quantitative nanomechanical mapping of DMT modulus simultaneously (Figure 7a–c) when imaging the topography of samples at high resolution. Due to EP and PU have disparate mechanical properties at room temperature; quantitative nanomechanical property mapping is quite suitable for detection of phase distribution in the gradient IPN [17,46,47]. Fracture surface of the gradient composite was prepared as the same in the contact angle measurement.

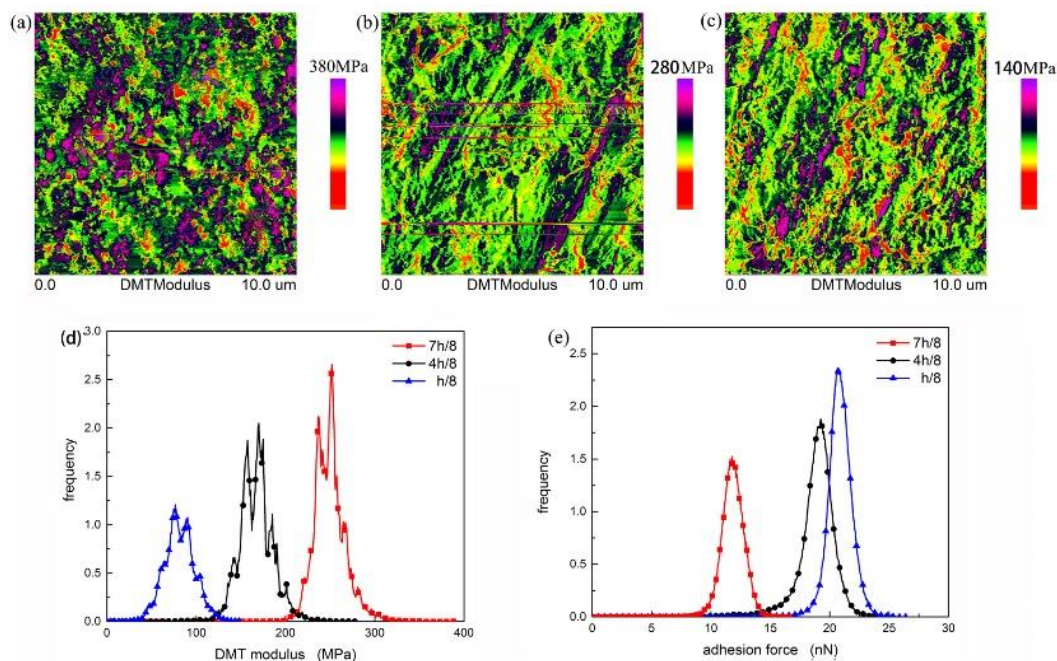


Figure 7. Quantitative nanomechanical property mapping images for 7/8 h (a), 4/8 h (b) and 1/8 h (c) of the continuous gradient IPN composite. The modulus images were taken after an absolute calibration process. Distribution histogram of the Derjaguin–Muller–Toporov (DMT) modulus (d) and adhesive force (e) at the corresponding selection regions.

As shown in Figure 7a–c, there are layer structures along the gradient direction. The DMT modulus (Figure 7d) of the three selected region are 80 ± 40 MPa (7/8 h), 160 ± 55 MPa (4/8 h) and 255 ± 55 MPa (1/8 h), respectively, which increases along with the gradient direction from bottom to top of the IPN structure. While, the adhesion force (Figure 7e) of the three selected region are 21 ± 3 nN (7/8 h), 19 ± 4 nN (4/8 h) and 12 ± 3 nN (1/8 h), respectively, which decreases along with the gradient direction from bottom to top of the IPN structure. This results from the earlier gelled PU phase moving toward to the bottom in the solidifying process, meanwhile the EP phase was extruded to the top of this IPN. This progress would have been frozen before a complete phase separation, which leads to the generation of the gradient structure.

3.6. DMA Analysis

Damping curves of EP, PU and the three kinds of IPN materials are shown in Figure 8.

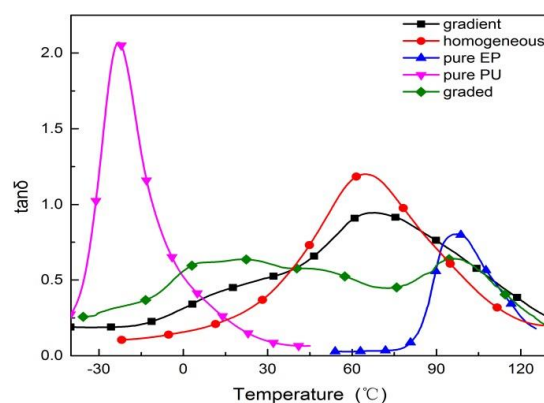


Figure 8. Damping curves of the EP, PU and the three kinds of IPN materials. Specimens were measured under the shear mode from -40 to 130 °C with a heating rate of 1.5 °C/min. Specimen dimension were $\Phi 8.79$ mm \times 2.17 mm.

The best damping performance of EP and PU appears at -19.5 and 97.6 °C, respectively, thus they are not suitable for using alone. The IPN modification technology is one of the most widely used methods for polymer modification. As is shown in Figure 8, the damping temperature ΔT (in which loss factor value is larger than 0.3) of the homogeneous IPN locates in the range of 23.2 – 116.7 °C with a distinct peak (value: 1.21) at 65.8 °C, which can be used as traditional polymer damping material. However, though the damping temperature ΔT of this homogeneous IPN has been shifted into the general service temperature regions, their storage modules are not high enough to provide the self-supporting strength within the ΔT . The common improvement is pasting several IPN layers with different T_g together, which is named the graded IPN. DMA curves show that the damping temperature range of this graded IPN is from -25.8 to 120.7 °C, which is wider than the other IPNs. However, the $\tan\delta$ of this graded IPN is less than 0.65, which is lower than others. What is more interesting, the gradient IPN has a good balance between the damping temperature range and the loss factor. It is suitable for using as a self-supporting damping structure which can provide self-supporting strength and keep its shape in working temperatures. When the soft side is pasted to substrates and the hard surface is exposed outside, this kind of structure can be used as a replacement of constrained damping structure, reducing stress concentration and risk of joint failure [48]. Besides, comparing to the graded IPN composite, the fabricating method of the gradient IPN is simplified.

There are three reasons that are responsible for the good damping performance of this continuous gradient IPN composite.

Firstly, interface friction is the main factor to influence the damping property [49]. Numbers of the interfaces are directly affected by the solubility of the components. Because of the relatively poor

compatibility of the resins, phase separation (Figure 7) of the IPN would occur unavoidably and result in a multiphase structure

Secondly, curing reactions of the components happen immediately the time when resins are mixed. The mixed resins will gel and cure before the complete phase separation, creating the gradient structure. The gradient IPN can be regarded as a kind of composite stacked up together by “infinite layers of IPN materials” [50,51] (as is shown in Figure 7, especially in Figure 7c). Each “IPN layer” has different glass transition temperatures (T_g), and those T_g points transit from the glass transition temperature of PU to that of EP. Due to the “transition regions” in the gradient composite always exist and transfer along with the temperature change, this gradient composite show better damping performances comparing to homogeneous polymers. Besides, as is shown in Figure 7, there are innumerable phase running through the adjacent layers. Under a certain temperature, one “IPN layer” may be under its T_g point while the other nearby is not; hence even the adjacent layers also have different responses during vibration. Phase that going across the adjacent layers will increase the vibration friction greatly [52]. Friction exists not only in each layer, but also in the adjacent layers.

Thirdly, the good damping properties of the gradient IPN composite can also be explained by the molecular structure. Ether bond and carbon-carbon bond in resins have lower barrier potential and are more flexible when compared to the rigid phenyl, urethane, allophanate and biuret group, etc. [53]. In IPN structure, the flexible bonds are restricted by the rigid chains. Because of the forced miscibility among the molecular chains, IPNs have greater friction force during vibrations than single component polymers [54]. Furthermore, there exist innumerable hydrogen bond between the polar molecules in the IPN structures, they undergo the bond crack and rebuilding during a vibration [55–57], and thus it would bring more energy dissipation.

As to the graded one, though it has a wider ΔT comparing to the others, there are only six layers of IPNs existing and each layer has a relative large different responses to vibrations. On the one hand, the discrepant stiffness would restrict deformation and then the spread of vibration energy, which would decrease the energy dissipation. On the other hand, there would be only one layer has the best damping performance under a certain temperature in the graded IPN composite, but this layer would devote only a small part to the whole sample’s damping performance. In a word, the continuous gradient IPN has the best damping performance when compared to the others.

4. Conclusions

We have prepared a gradient distributing IPN composite using EP and PU simply and inexpensively. We adopted UV-vis, TG, DSC, DMA, AFM and water contact angle to characterize this IPN composite, and found that the absorption in visible light region, glass-transition temperatures (T_g), thermal decomposition temperatures (T_d) and DMT modulus were increasing along with the gradient direction from bottom side to top side of the IPN. While the absorption in ultraviolet region and adhesion force were decreasing along with the gradient direction from the bottom side to the top side of the IPN. DMA analysis demonstrates that this continuous gradient IPN has a good balance between the damping temperature range and the loss factor which is suitable for using as a self-supporting damping structure.

Compared to the traditional homogeneous IPN composites, these gradient IPNs with different shapes and thicknesses can be created simply by adjusting the shape of the mold, the pre-curing temperature and the pre-curing time. Due to the gradually changing modulus, this IPN composite has the potential to replace the constrained damping materials by direct generation on substrates. This gradient composite will minimize the mismatch of the abrupt interfacial tension changes and reduce the adhesion failures of damping structures. The service life of these damping structures will be greatly lengthened.

Supplementary Materials: The following are available online at www.mdpi.com/2076-3417/7/2/135/s1, Figure S1: Schematic illustrations of the graded/bilayer/gradient materials, (a) the graded materials; (b) the bilayer material; (c) the gradient material, Figure S2: Relationship between the procuring time and the gradient structures.

The component ratio EP/PU = 60/40. Procuring temperature is 10 °C. (a) Pre-cured for 0.5 h; (b) pre-cured for 24 h; (c) pre-cured for 48h, Figure S3: SEM picture of the gradient IPN composite (PU/EP = 40/60), Figure S4: Scanning electron microscopy/energy-dispersive X-ray technique (SEM-EDX) analysis of the 70/30 (EP/PU) gradient material. Figure S4a is the fracture surface of the gradient material. Figure S4b is the nitrogen distribution of Figure S4a and the chosen region for the element content analysis. Figure S4c is the whole nitrogen content of the fracture surface. Figure S4d, Figure S4e and Figure S4f are the detailed data of the chosen regions in Figure S4b, Figure S5: ATR-FTIR results of the chosen regions of the gradient sample. Devices applied here have been revised before detection and all curves here have subtracted the baseline, Figure S6: FTIR spectra of the locations chosen from the homogeneous IPN, Table S1: Element distribution of the selected slices from the sample.

Acknowledgments: This work supported by the Fundamental Research Funds for the Central Universities (WUT: 2017IVA093).

Author Contributions: Xuesong Lv and Zhixiong Huang were responsible for the designing of the experiments; Xuesong Lv performed the whole experiments; Guanbin Gao and Wenrui Chen carried out the AFM and UV-vis test; Xuesong Lv and Minxian Shi analyzed the experimental data; Xuesong Lv, Yun Fan and Guanbin Gao wrote the whole paper.

Conflicts of Interest: The authors declare no conflict of interest. The founding sponsors had no role in the design of the study; in the collection, analyses, or interpretation of data; in the writing of the manuscript, and in the decision to publish the results.

References

1. Tian, S.; Cui, F.; Wang, X. New type of piezo-damping epoxy-matrix composites with multi-walled carbon nanotubes and lead zirconate titanate. *Mater. Lett.* **2008**, *62*, 3859–3861. [[CrossRef](#)]
2. Gusev, A.A.; Feldman, K.; Guseva, O. Using Elastomers and Rubbers for Heat-Conduction Damping of Sound and Vibrations. *Macromolecules* **2010**, *43*, 2638–2641. [[CrossRef](#)]
3. Li, G.; Ma, Y.; He, X.; Li, W.; Li, P. Damping capacity of high strength-damping aluminum alloys prepared by rapid solidification and powder metallurgy process. *Tans. Nonferr. Metals Soc. China* **2012**, *22*, 1112–1117. [[CrossRef](#)]
4. Zahedi, F.; Amraei, I.A.; Fathizade, M.A. Investigation of dynamic-mechanical properties of multilayer latex IPNs (MLIPNs) with core/shell morphology: Synthesis and characterization. *Polymer* **2016**, *83*, 162–171. [[CrossRef](#)]
5. Recho, P.; Ranft, J.; Marcq, P. One-dimensional collective migration of a proliferating cell monolayer. *Soft Matter* **2016**, *12*, 2381–2391. [[CrossRef](#)] [[PubMed](#)]
6. Qin, C.L.; Zhao, D.Y.; Bai, X.D.; Zhang, X.G.; Zhang, B.; Jin, Z.; Niu, H.J. Vibration damping properties of gradient polyurethane/vinyl ester resin interpenetrating polymer network. *Mater. Chem. Phys.* **2006**, *97*, 517–524. [[CrossRef](#)]
7. Song, M.; Zhao, X.; Li, Y.; Hu, S.; Zhang, L.; Wu, S. Molecular dynamics simulations and microscopic analysis of the damping performance of hindered phenol AO-60_nitrile-butadiene rubber composites. *RSC Adv.* **2014**, *4*, 6719–6729. [[CrossRef](#)]
8. Senake Perera, M.C.; Ishiaku, U.S.; Mohd Ishak, Z.A. Characterisation of PVC/NBR and PVC/ENR50 binary blends and PVC/ENR50/NBR ternary blends by DMA and solid state NMR. *Eur. Polym. J.* **2001**, *37*, 167–178. [[CrossRef](#)]
9. Lin, C.; Kuo, S.; Huang, C.; Chang, F. Glass transition temperature enhancement of PMMA through copolymerization with PMAAM and PTCM mediated by hydrogen bonding. *Polymer* **2010**, *51*, 883–889. [[CrossRef](#)]
10. Ungar, E.E. Loss Factors of Viscoelastically Damped Beam Structures. *J. Acoust. Soc. Am.* **1962**, *34*, 1082–1089. [[CrossRef](#)]
11. Knapp, G.; Oreski, G.; Pinter, G. Method to characterize the damping behavior of thin passively constrained layer laminates using dynamic mechanical analysis (DMA) in shear mode. *Polym. Test.* **2015**, *42*, 215–224. [[CrossRef](#)]
12. Rao, M.D. Recent applications of viscoelastic damping for noise control in automobiles and commercial airplanes. *J. Sound Vib.* **2003**, *262*, 457–474. [[CrossRef](#)]
13. Lee, W.; Han, S.; Park, W. A refined higher order shear and normal deformation theory for E-, P-, and S-FGM plates on Pasternak elastic foundation. *Compos. Struct.* **2015**, *122*, 330–342. [[CrossRef](#)]

14. Pradhan, K.K.; Chakraverty, S. Static analysis of functionally graded thin rectangular plates with various boundary supports. *Arch. Civ. Mech. Eng.* **2015**, *15*, 721–734. [[CrossRef](#)]
15. Koizumi, M. FGM activities in Japan. *Compos. Part B Eng.* **1997**, *28*, 1–4. [[CrossRef](#)]
16. Dubey, A.K.; Kakimoto, K.; Obata, A.; Kasuga, T. Enhanced polarization of hydroxyapatite using the design concept of functionally graded materials with sodium potassium niobate. *RSC Adv.* **2014**, *4*, 24601–24611. [[CrossRef](#)]
17. Lambros, J.; Santare, M.H.; Li, H.; Sapna, G.H., III. A Novel Technique for the Fabrication of Laboratory Scale Model Functionally Graded Materials. *Exp. Mech.* **1999**, *3*, 184–190. [[CrossRef](#)]
18. Tang, Z.; Wang, Y.; Podsiadlo, P.; Kotov, N.A. Biomedical Applications of Layer-by-Layer Assembly: From Biomimetics to Tissue Engineering. *Adv. Mater.* **2006**, *18*, 3203–3224. [[CrossRef](#)]
19. De Villiers, M.M.; Otto, D.P.; Strydom, S.J.; Lvov, Y.M. Introduction to nanocoatings produced by layer-by-layer (LbL) self-assembly. *Adv. Drug Deliv. Rev.* **2011**, *63*, 701–715. [[CrossRef](#)] [[PubMed](#)]
20. Lin-Gibson, S.; Landis, F.A.; Drzal, P.L. Combinatorial investigation of the structure-properties characterization of photopolymerized dimethacrylate networks. *Biomaterials* **2006**, *27*, 1711–1717. [[CrossRef](#)] [[PubMed](#)]
21. Crowe-Willoughby, J.A.; Weiger, K.L.; Özçam, A.E.; Genzer, J. Formation of silicone elastomer networks films with gradients in modulus. *Polymer* **2010**, *51*, 763–773. [[CrossRef](#)]
22. Kloxin, A.M.; Benton, J.A.; Anseth, K.S. In situ elasticity modulation with dynamic substrates to direct cell phenotype. *Biomaterials* **2010**, *31*, 1–8. [[CrossRef](#)] [[PubMed](#)]
23. Zaari, N.; Rajagopalan, P.; Kim, S.K.; Engler, A.J.; Wong, J.Y. Photopolymerization in Microfluidic Gradient Generators: Microscale Control of Substrate Compliance to Manipulate Cell Response. *Adv. Mater.* **2004**, *16*, 2133–2137. [[CrossRef](#)]
24. Honma, T.; Zhao, L.; Asakawa, N.; Inoue, Y. Poly(ϵ -Caprolactone)/Chitin and Poly(ϵ -Caprolactone)/Chitosan Blend Films With Compositional Gradients: Fabrication and Their Biodegradability. *Macromol. Biosci.* **2006**, *6*, 241–249. [[CrossRef](#)] [[PubMed](#)]
25. Förster, N.; Pöppler, A.; Stalke, D.; Vana, P. Photocrosslinkable Star Polymers via RAFT-Copolymerizations with *N*-Ethylacrylate-3,4-dimethylmaleimide. *Polymers* **2013**, *5*, 706–729. [[CrossRef](#)]
26. Lai, E.; Wang, Y.; Wei, Y.; Li, G. Preparation of Uniform-Sized and Dual Stimuli-Responsive Microspheres of Poly(*N*-Isopropylacrylamide)/Poly(Acrylic acid) with Semi-IPN Structure by One-Step Method. *Polymers* **2016**, *8*, 90. [[CrossRef](#)]
27. Suresh, S. Graded materials for resistance to contact deformation and damage. *Science* **2001**, *292*, 2447–2451. [[CrossRef](#)] [[PubMed](#)]
28. Lipatov, Y.S.; Karbanova, L.V. Review: Gradient interpenetrating polymer networks. *J. Appl. Sci.* **1995**, *30*, 2475–2484.
29. Liu, B.L.; Wang, J.B.; Zhong, X.L.; Huang, K.; Li, B.; Wang, F.; Xie, J.; Zhou, Y.C. Enhanced electrocaloric effect in a Ba(1-x)Sr_xTiO₃ compositionally graded film. *RSC Adv.* **2014**, *4*, 24533–24537. [[CrossRef](#)]
30. Lin, Y.; Minner, D.; Herring, V.; Naumann, C. Physisorbed Polymer-Tethered Lipid Bilayer with Lipopolymer Gradient. *Materials* **2012**, *5*, 2243–2257. [[CrossRef](#)]
31. Carr, L.R.; Krause, J.E.; Ella-Menye, J.; Jiang, S. Single nonfouling hydrogels with mechanical and chemical functionality gradients. *Biomaterials* **2011**, *32*, 8456–8461. [[CrossRef](#)] [[PubMed](#)]
32. Thomopoulos, S.; Williams, G.R.; Gimbel, J.A.; Favata, M.; Soslowsky, L.J. Variation of biomechanical, structural, and compositional properties along the tendon to bone insertion site. *J. Orthop. Res.* **2003**, *21*, 413–419. [[CrossRef](#)]
33. Miserez, A.; Schneberk, T.; Sun, C.J.; Zok, F.W.; Waite, J.H. The transition from stiff to compliant materials in squid beaks. *Science* **2008**, *319*, 1816–1819. [[CrossRef](#)] [[PubMed](#)]
34. Coyne, K.J.; Waite, J.H. In search of molecular dovetails in mussel byssus: From the threads to the stem. *J. Exp. Biol.* **2000**, *203*, 1425–1431. [[PubMed](#)]
35. Moeser, G.M. Seasonal variation in mussel byssal thread mechanics. *J. Exp. Biol.* **2006**, *209*, 1996–2003. [[CrossRef](#)] [[PubMed](#)]
36. Claussen, K.U.; Scheibel, T.; Schmidt, H.; Giesa, R. Polymer Gradient Materials: Can Nature Teach Us New Tricks? *Macromol. Mater. Eng.* **2012**, *297*, 938–957. [[CrossRef](#)]
37. Tamarin, A.; Lewis, P.; Askey, J. The structure and formation of the byssus attachment plaque in *Mytilus*. *J. Morphol.* **1976**, *149*, 199–221. [[CrossRef](#)] [[PubMed](#)]

38. Lv, X.; Huang, Z.; Huang, C.; Shi, M.; Gao, G.; Gao, Q. Damping properties and the morphology analysis of the polyurethane/epoxy continuous gradient IPN materials. *Compos. Part B Eng.* **2016**, *88*, 139–149. [[CrossRef](#)]
39. Workman, J., Jr. *The Handbook of Organic Compounds, Three-Volume Set: NIR, IR, R, and UV-Vis Spectra Featuring Polymers and Surfactants*; Academic Press: Cambridge, MA, USA, 2000; Volume 2016, p. 1493.
40. Sojka, Z.; Bozon-Verduraz, F.; Che, M. *UV-Vis-NIR and EPR Spectroscopies*; Wiley-VCH Verlag GmbH & Co. KGaA: Weinheim, Germany, 2008.
41. Llewellyn, E.J.; Lloyd, N.D.; Degenstein, D.A.; Gattinger, R.L.; Petelina, S.V.; Bourassa, A.E.; Wiensz, J.T.; Ivanov, E.V.; McDade, I.C.; Solheim, B.H.; et al. The OSIRIS instrument on the Odin spacecraft. *Can. J. Phys.* **2004**, *82*, 411–422. [[CrossRef](#)]
42. Owens, D.K.; Wendt, R.C. Estimation of the surface free energy of polymers. *Appl. Polym. Sci.* **1969**, *8*, 1741–1747. [[CrossRef](#)]
43. Meiron, T.S.; Marmur, A.; Saguy, I.S. Contact angle measurement on rough surfaces. *J. Colloid Interface Sci.* **2004**, *274*, 637–644. [[CrossRef](#)] [[PubMed](#)]
44. Packham, D.E. Surface energy, surface topography and adhesion. *Int. J. Adhes. Adhes.* **2003**, *23*, 437–448. [[CrossRef](#)]
45. Mattozzi, A.; Hedenqvist, M.S.; Gedde, U.W. Diffusivity of n-hexane in poly(ethylene-stat-octene)s assessed by molecular dynamics simulation. *Polymer* **2007**, *48*, 5174–5180. [[CrossRef](#)]
46. Bergman, J.A.; Cochran, E.W.; Heinen, J.M. Role of the segment distribution in the microphase separation of acrylic diblock and triblock terpolymers. *Polymer* **2014**, *55*, 4206–4215. [[CrossRef](#)]
47. Wang, Q.; Chen, S.; Wang, T.; Zhang, X. Damping, thermal, and mechanical properties of polyurethane based on poly(tetramethylene glycol)/epoxy interpenetrating polymer networks: Effects of composition and isocyanate index. *Appl. Phys. A* **2011**, *104*, 375–382. [[CrossRef](#)]
48. Gao, G.; Zhang, M.; Lu, P.; Guo, G.; Wang, D.; Sun, T. Chirality-assisted ring-like aggregation of A β (1–40) at liquid–solid interfaces: A stereoselective two-step assembly process. *Angew. Chem. Int. Ed.* **2015**, *54*, 2245–2250. [[CrossRef](#)] [[PubMed](#)]
49. Xu, K.; Zhang, F.; Zhang, X.; Guo, J.; Wu, H.; Guo, S. Molecular insights into the damping mechanism of poly(vinyl acetate)/hindered phenol hybrids by a combination of experiment and molecular dynamics simulation. *RSC Adv.* **2015**, *5*, 4200–4209. [[CrossRef](#)]
50. Wang, P.Y.; Clements, L.R.; Thissen, H.; Tsai, W.B.; Voelcker, N.H. Screening rat mesenchymal stem cell attachment and differentiation on surface chemistries using plasma polymer gradients. *Acta Biomater.* **2015**, *11*, 58–67. [[CrossRef](#)] [[PubMed](#)]
51. Sperling, L.H.; Frideman, D.W. Synthesis and mechanical behavior of interpenetrating polymer network. *J. Appl. Polym. Sci.* **1969**, *7*, 425–427.
52. Zhao, X.; Xiang, P.; Tian, M.; Fong, H.; Jin, R.; Zhang, L. Nitrile butadiene rubber/hindered phenol nanocomposites with improved strength and high damping performance. *Polymer* **2007**, *48*, 6056–6063. [[CrossRef](#)]
53. Peter, C.; Kremer, K. Multiscale simulation of soft matter systems—From the atomistic to the coarse-grained level and back. *Soft Matter* **2009**, *5*, 4357. [[CrossRef](#)]
54. Sorathia, U.; Yeager, W.; Dapp, T. Advanced Damping Materials for Marine Applications. In *Sound and Vibration Damping with Polymers*; American Chemical Society: Washington, DC, USA, 1990; pp. 382–396.
55. Wu, C.; Yamagishi, T.; Nakamoto, Y.; Ishida, S.; Nitta, K.; Kubota, S. Organic hybrid of chlorinated polyethylene and hindered phenol. I. Dynamic mechanical properties. *J. Polym. Sci. Part B Polym. Phys.* **2000**, *38*, 2285–2295. [[CrossRef](#)]
56. Wu, P.; Yang, Y.; Siesler, H.W. Two-dimensional near-infrared correlation temperature studies of an amorphous polyamide. *Polymer* **2001**, *42*, 10181–10186. [[CrossRef](#)]
57. Kim, S.H.; Tan, J.P.K.; Nederberg, F.; Fukushima, K.; Colson, J.; Yang, C.; Nelson, A.; Yang, Y.; Hedrick, J.L. Hydrogen bonding-enhanced micelle assemblies for drug delivery. *Biomaterials* **2010**, *31*, 8063–8071. [[CrossRef](#)] [[PubMed](#)]

